Atlas of Formability

Super α_2 Titanium Aluminides

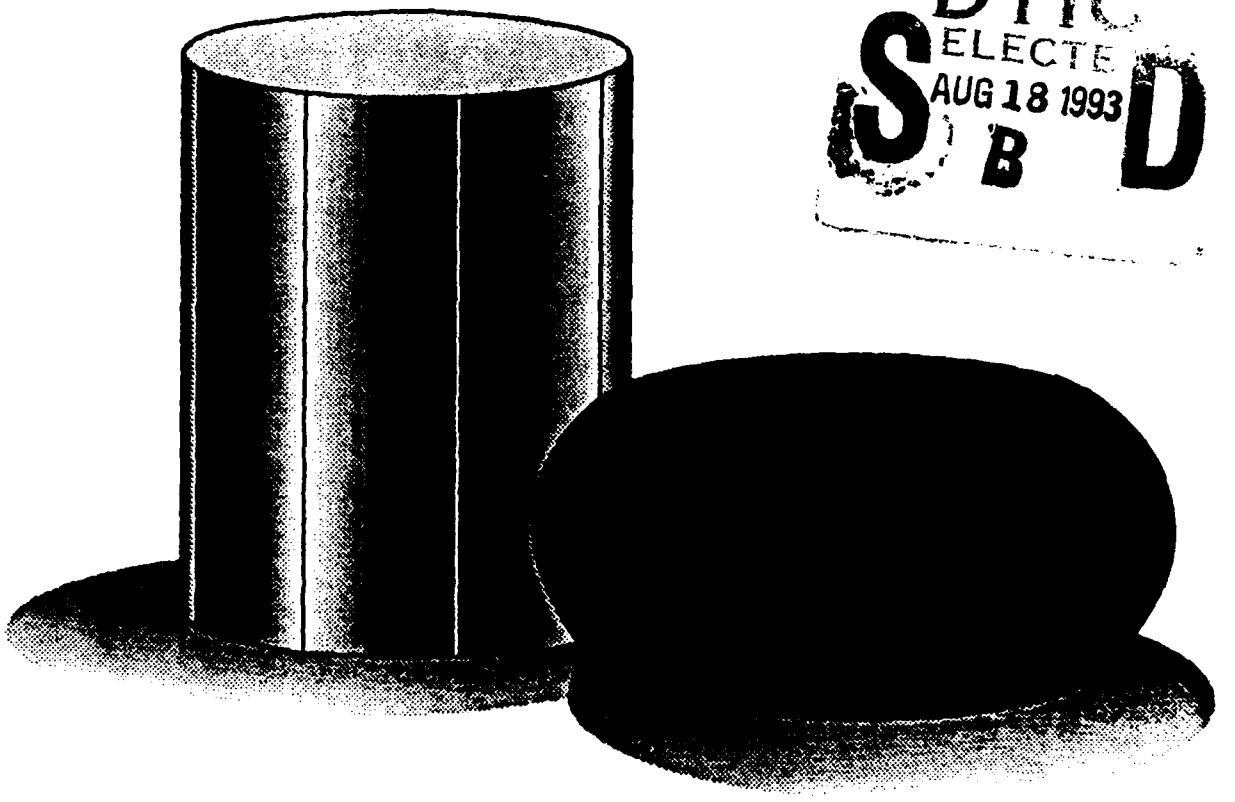

NCEMT

DISCLAIMER NOTICE

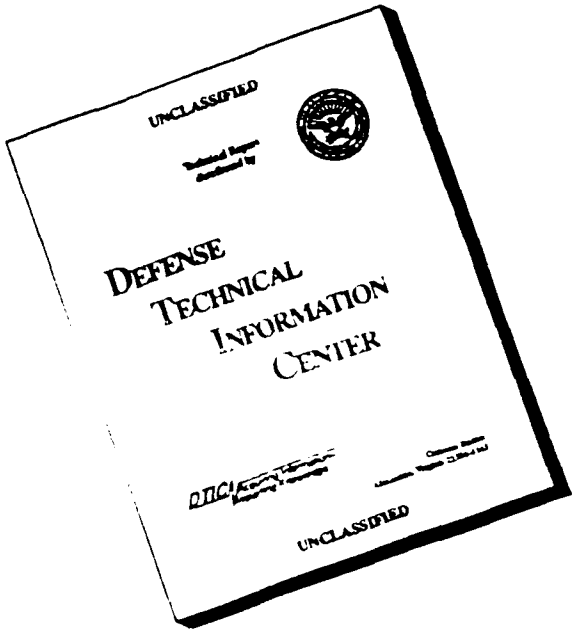

THIS DOCUMENT IS BEST QUALITY AVAILABLE. THE COPY FURNISHED TO DTIC CONTAINED A SIGNIFICANT NUMBER OF PAGES WHICH DO NOT REPRODUCE LEGIBLY.

ATLAS OF FORMABILITY

SUPER α_2 TITANIUM ALUMINIDE

by

Prabir K. Chaudhury and Dan Zhao

National Center for Excellence in Metalworking Technology
1450 Scalp Avenue
Johnstown, PA 15904

for

Naval Industrial Resource Support Activity
Building 75-2, Naval Base
Philadelphia, PA 19112-5078

June 30, 1992

REPORT DOCUMENTATION PAGE

Form Approved
OMB No 0704-0188

1. AGENCY USE ONLY (Leave blank)	2. REPORT DATE	3. REPORT TYPE AND DATES COVERED
	June 30, 1992	Final, March 31, 1992 - June 30, 1992

4. TITLE AND SUBTITLE

ATLAS OF FORMABILITY
Super α_2 Titanium Aluminide

5. FUNDING NUMBERS

C-N00140-88-C-RC21

6. AUTHOR(S)

Prabir K. Chaudhury
Dan Zhao

7. PERFORMING ORGANIZATION NAME(S) AND ADDRESS(ES)

National Center for Excellence in Metalworking Technology (NCEMT)
1450 Scalp Avenue
Johnstown, PA 15904

8. PERFORMING ORGANIZATION REPORT NUMBER

9. SPONSORING / MONITORING AGENCY NAME(S) AND ADDRESS(ES)

Naval Industrial Resources Support Activity
Building 75-2, Naval Base
Philadelphia, PA 19112-5078

10. SPONSORING / MONITORING AGENCY REPORT NUMBER

11. SUPPLEMENTARY NOTES

12a. DISTRIBUTION / AVAILABILITY STATEMENT

12b. DISTRIBUTION CODE

13. ABSTRACT *(Maximum 200 words)*

In this investigation, flow behavior of Super α_2 titanium aluminide was studied by conducting compression tests over a wide range of temperatures and strain rates. Constitutive relations were determined from the flow behavior, and a dynamic material modeling was conducted on this alloy. Thus, the optimum processing condition in terms of temperature and strain rate was identified. Microstructural changes during high temperature deformation were also characterized.

14. SUBJECT TERMS

Super α_2, Deformation Processing, High Temperature Deformation, Processing Map, Metalworking, Microstructure

15. NUMBER OF PAGES

32

16. PRICE CODE

17. SECURITY CLASSIFICATION OF REPORT	18. SECURITY CLASSIFICATION OF THIS PAGE	19. SECURITY CLASSIFICATION OF ABSTRACT	20. LIMITATION OF ABSTRACT
Unclassified	Unclassified	Unclassified	

TABLE OF CONTENTS

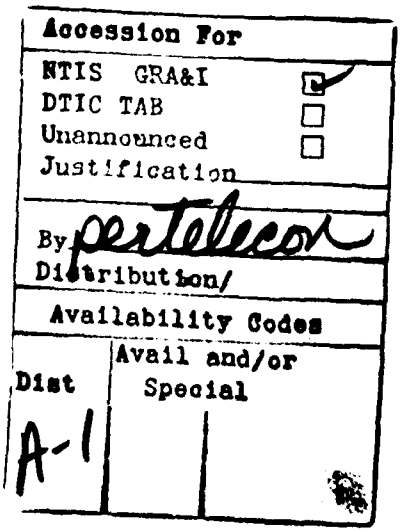

LIST OF TABLE

Super α_2 Titanium Aluminides

Introduction

Super α_2 titanium aluminides have attracted much attention in aircraft industry because of their light weight, high strength and stiffness, and high temperature resistance. Although this alloy was designed for improved mechanical properties in service, it exhibits low ductility at low temperatures and has limited workability compared to conventional titanium alloys. For successful manufacturing using this alloy it is desirable to find the mechanical as well as microstructural conditions at which the alloy can be processed with optimum efficiency. Flow behavior of the alloy through compression testing at various temperatures and strain rates were performed to determine the constitutive relation at high strain rates. From the constitutive relation a dynamic material modeling on super α_2 was carried out to optimize processing conditions such as temperature and strain rate. In addition, workability tests and microstructural characterizations were conducted to show the effect of the optimization on the formability and the resulting microstructure.

Experimental Procedure

The material used in this project was Ti-14Al-20Nb-3.2V-2Mo (wt%) produced by RMI Titanium Co. , Niles, Ohio. The materials were cast, forged, and hot rolled and was in the form of hot rolled plate with thickness of 0.782 and 0.804 inch. As-received microstructure is shown in Figure 1.

Both flow stress-strain testing and workability testing were carried out in compression with cylindrical specimens. The specimens had a diameter of 0.5 inches and a height of 0.625 inches. For flow stress-strain testing, the test matrix is as follows:

Temperature, C (F):	843 (1550), 899 (1650), 954 (1750), and 1010 (1850)
Strain rate, s^{-1}:	0.1, 2, 4, 6, and 8.

Workability tests was conducted at temperatures of 843 C (1550 F) and 1010 C (1850 F), and strain rate of 4 s^{-1}.

Microstructural analysis of the deformed specimens was conducted using scanning electron microscope (SEM) with backscattered electron image (BEI). Specimens were cut through the compression axis (longitudinal) and transverse direction, and micrographs were taken at the center of the specimens.

Results

All the true stress-true strain flow curves with corresponding microstructures are shown in Figures 2 to 20. Table 1 is a list of the figures, test conditions and the observed microstructure. True stress versus strain rate was plotted in log-log scale in Figure 21 at a true strain of 0.2. The slope of the plot gave the strain rate sensitivity **m**, which is not a constant over the range of strain rate tested. Log stress vs. 1/T at 0.2 true strain is shown in Figure 22. Processing map at this strain was developed for super α_2 (Figure 23).

The results for workability tests are shown in Figures 24 for specimens tested at 843 C, and Figure 25 at 1010 C. At 843 C, there were no tensile cracks observed on the surfaces of the specimens, but slip bands formed due to localized shear at some strain combinations. As temperature was increased to 1010 C, workability increased extensively.

Table 1. List of figures, testing conditions and microstructural observations.

Figure No	Temperature F (C)	Strain Rate S^{-1}	Microstructure Backscattering Images (BEI)	Page No
1			As-received ($\alpha_2+\beta$) hot rolled plate.	3
2	1550 (843)	0.1	Elongated α_2 stringers in a ($\alpha_2+\beta$) matrix, where α_2 shows an elongated plate morphology, (longitudinal view).	4
3	1550 (843)	2.0	Same as above, but α_2 stringers are slightly larger, (longitudinal view).	5
4	1550 (843)	6.0	Same as above, but α_2 plates in the ($\alpha_2+\beta$) matrix are finer, (transverse view).	6
5	1550 (843)	8.0	Same as above, but α_2 stringers and the α_2 plates in the ($\alpha_2+\beta$) matrix are finer.	7
6	1650 (899)	0.1	Same as above, but the α_2 stringers and α_2 plates in the ($\alpha_2+\beta$) matrix are coarser at this temperature, (transverse view).	8
7	1650 (899)	2.0	Same as above, but the α_2 stringers have decreased in aspect ratio, (transverse view).	9
8	1650 (899)	4.0	Same as above, but the α_2 plates from the matrix appear more elongated, (transverse view).	10
9	1650 (899)	6.0	Same as above, but the α_2 stringers increased in aspect ratio, (transverse view).	11
10	1650 (899)	8.0	Similar to microstructures 9, (transverse view).	12
11	1750 (954)	0.1	Small and rod-like α_2 stringers and elongated plates of α_2 plates in the ($\alpha_2+\beta$) matrix, (longitudinal view).	13
12	1750 (954)	2.0	Same as above, (longitudinal view).	14
13	1750 (954)	4.0	Coarse and elongated α_2 stringers, (transverse view).	15
14	1750 (954)	6.0	Same as above, (transverse view).	16
15	1750 (954)	8.0	Flat stringers of α_2 in fine ($\alpha_2+\beta$) matrix, (longitudinal view)..	17
16	1850 (1010)	0.1	Large aspect ratio rod-like α_2 stringers in a ($\alpha_2+\beta$) matrix, where the proportion of α_2 is decreasing, (longitudinal view).	18
17	1850 (1010)	2.0	Same as above, but the α_2 phase in the ($\alpha_2+\beta$) matrix is very fine and decreasing in proportion, (longitudinal view).	19
18	1850 (1010)	4.0	Coarse and elongated α_2 stringers the α_2 phase in the ($\alpha_2+\beta$) matrix is becoming coarser, (transverse view).	20
19	1850 (1010)	6.0	Coarse and elongated α_2 stringers the α_2 phase in the ($\alpha_2+\beta$) matrix is becoming coarser, (transverse view).	21
20	1850 (1010)	8.0	Same as microstructure 17, (longitudinal view).	22

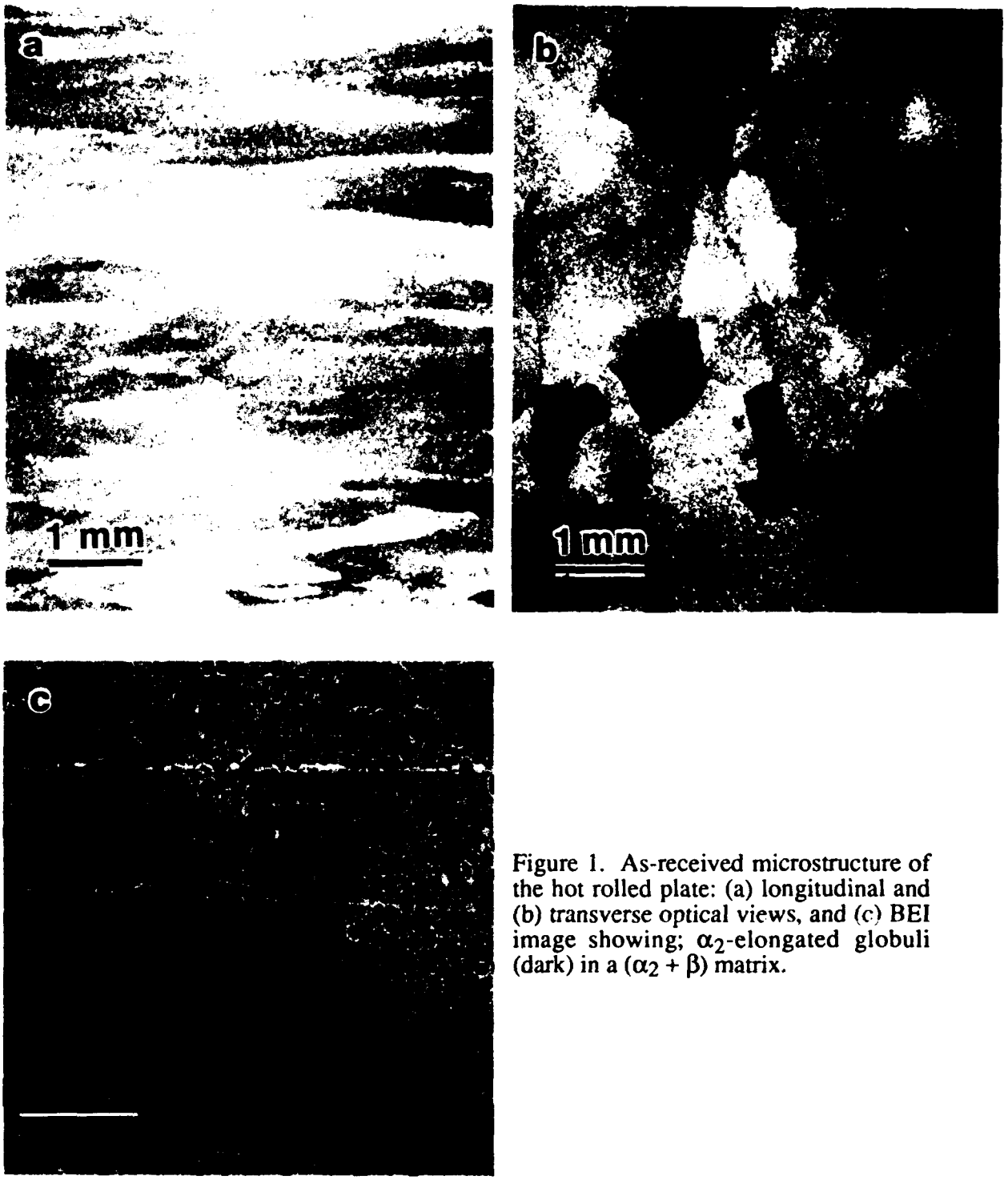

Figure 1. As-received microstructure of the hot rolled plate: (a) longitudinal and (b) transverse optical views, and (c) BEI image showing; α_2-elongated globuli (dark) in a (α_2 + β) matrix.

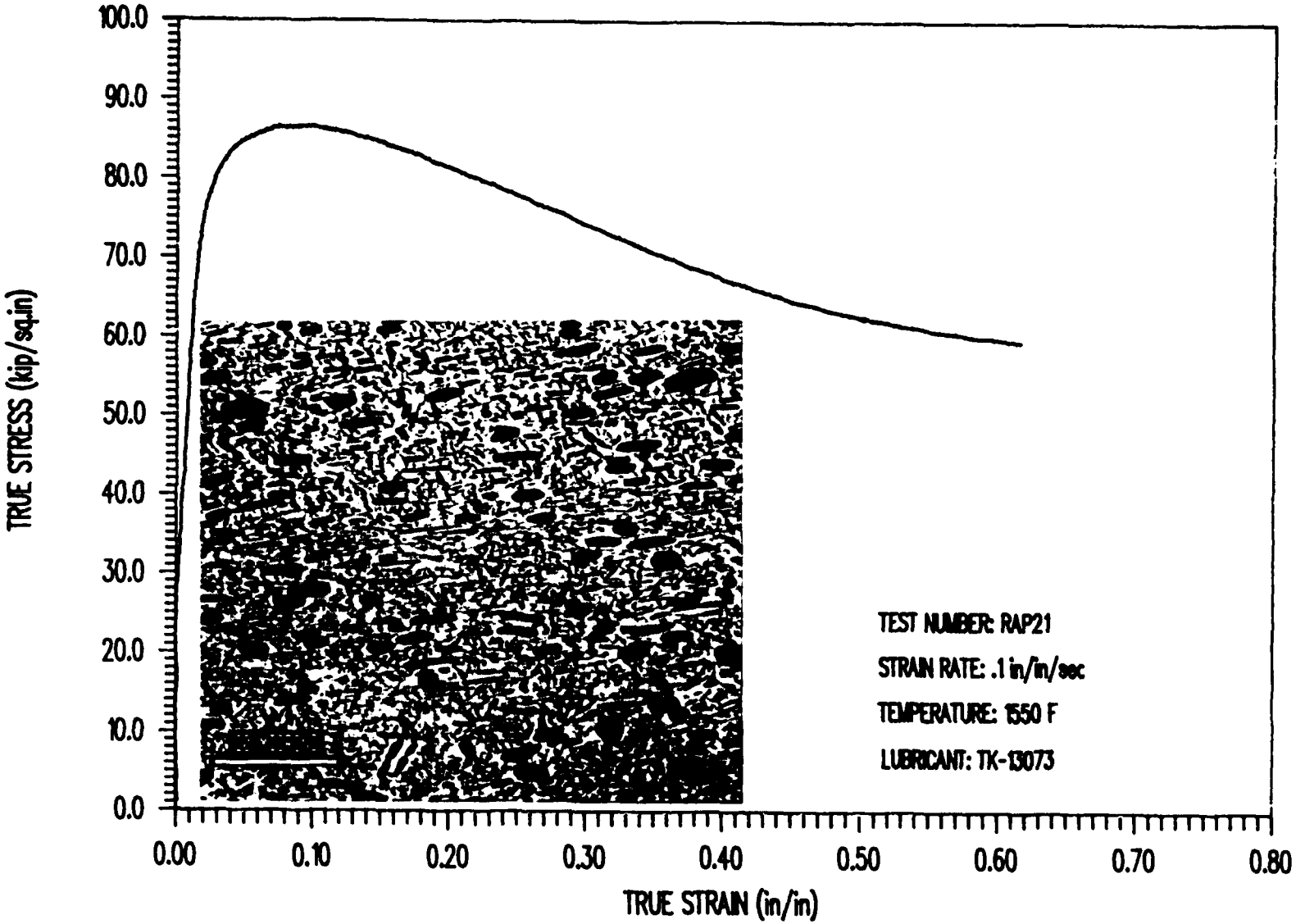

Figure 2. Compression true stress-true strain curve performed at 1550 F (843 C) and at a strain rate of 0.1 s^{-1}. The microstructure is a BEI view from the longitudinal axis of the specimen.

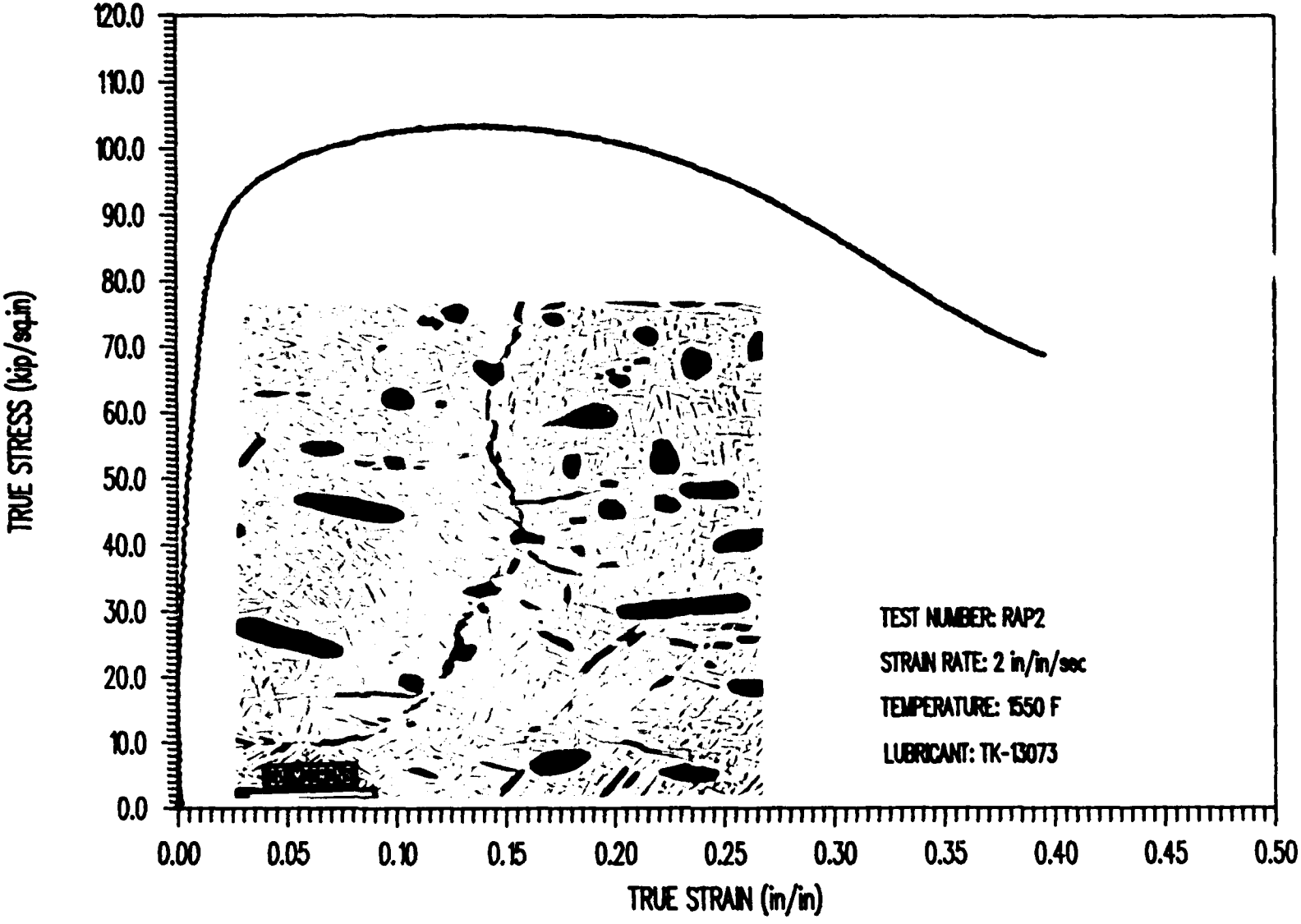

Figure 3. Compression true stress-true strain curve performed at 1550 F (843 C) and at a strain rate of 2.0 s^{-1}. The microstructure is a BEI view from the longitudinal axis of the specimen.

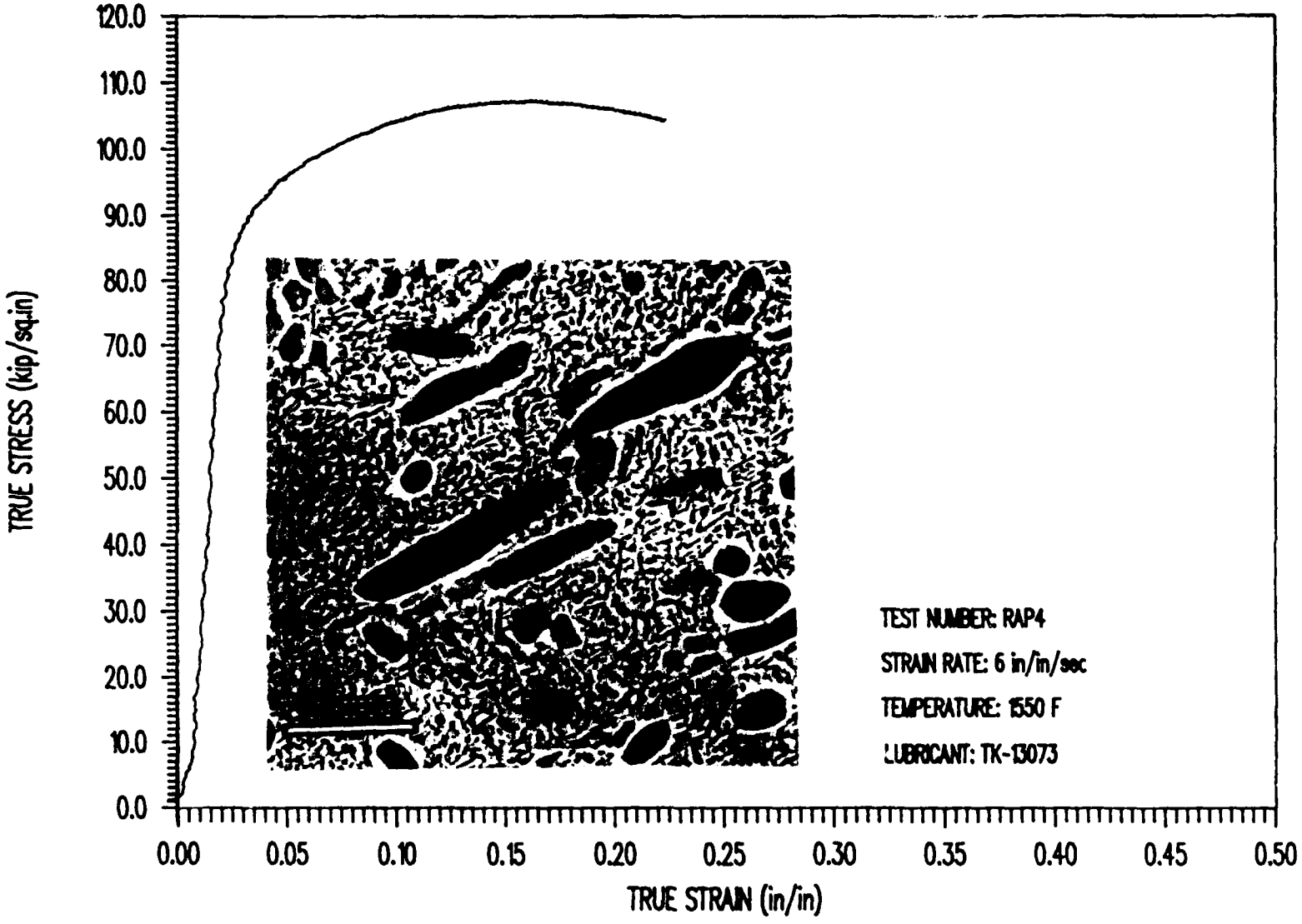

Figure 4. Compression true stress-true strain curve performed at 1550 F (843 C) and at a strain rate of 6.0 s^{-1}. The microstructure is a BEI view from the transverse axis of the specimen.

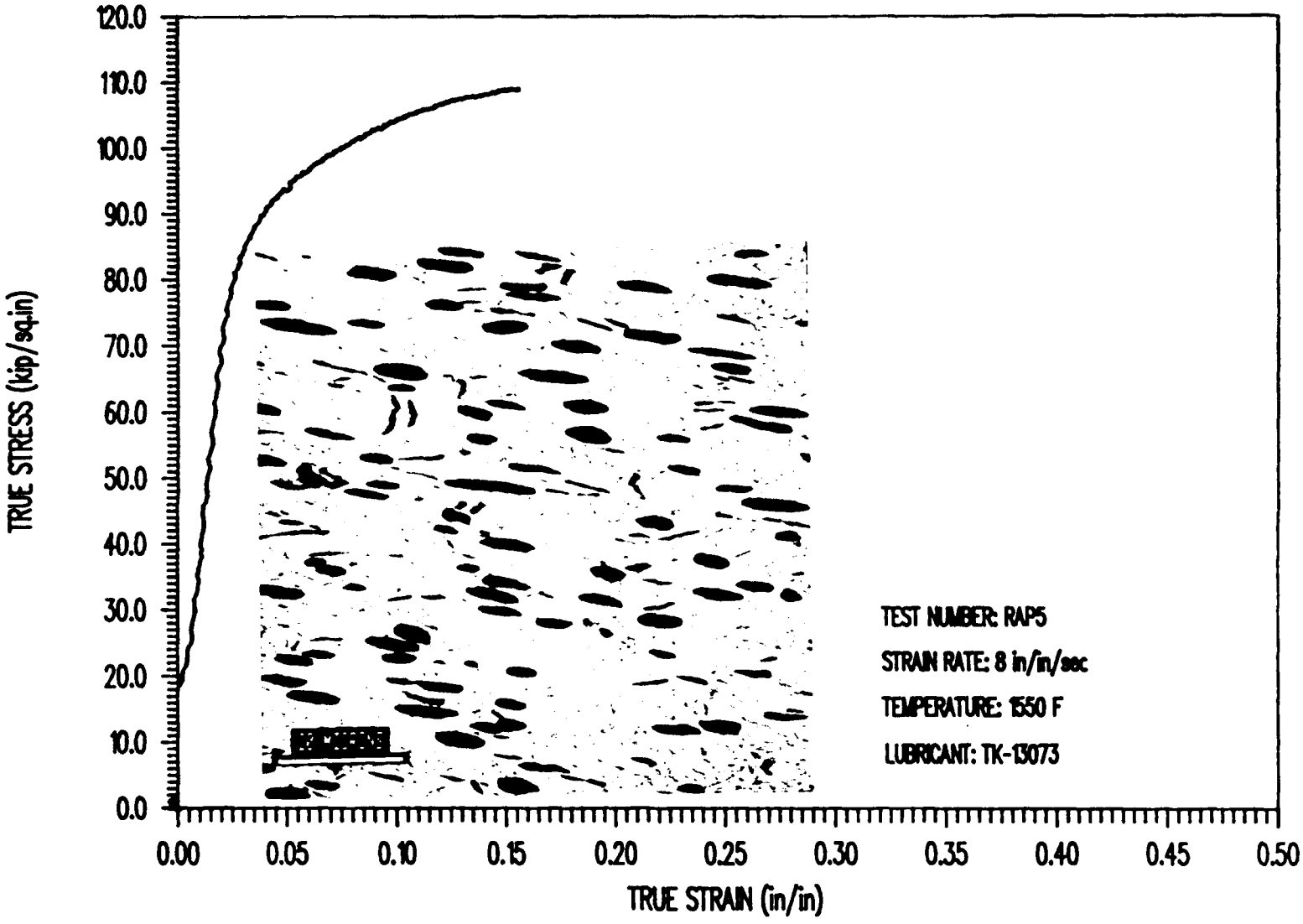

Figure 5. Compression true stress-true strain curve performed at 1550 F (843 C) and at a strain rate of 8.0 s^{-1}. The microstructure is a BEI view from the longitudinal axis of the specimen.

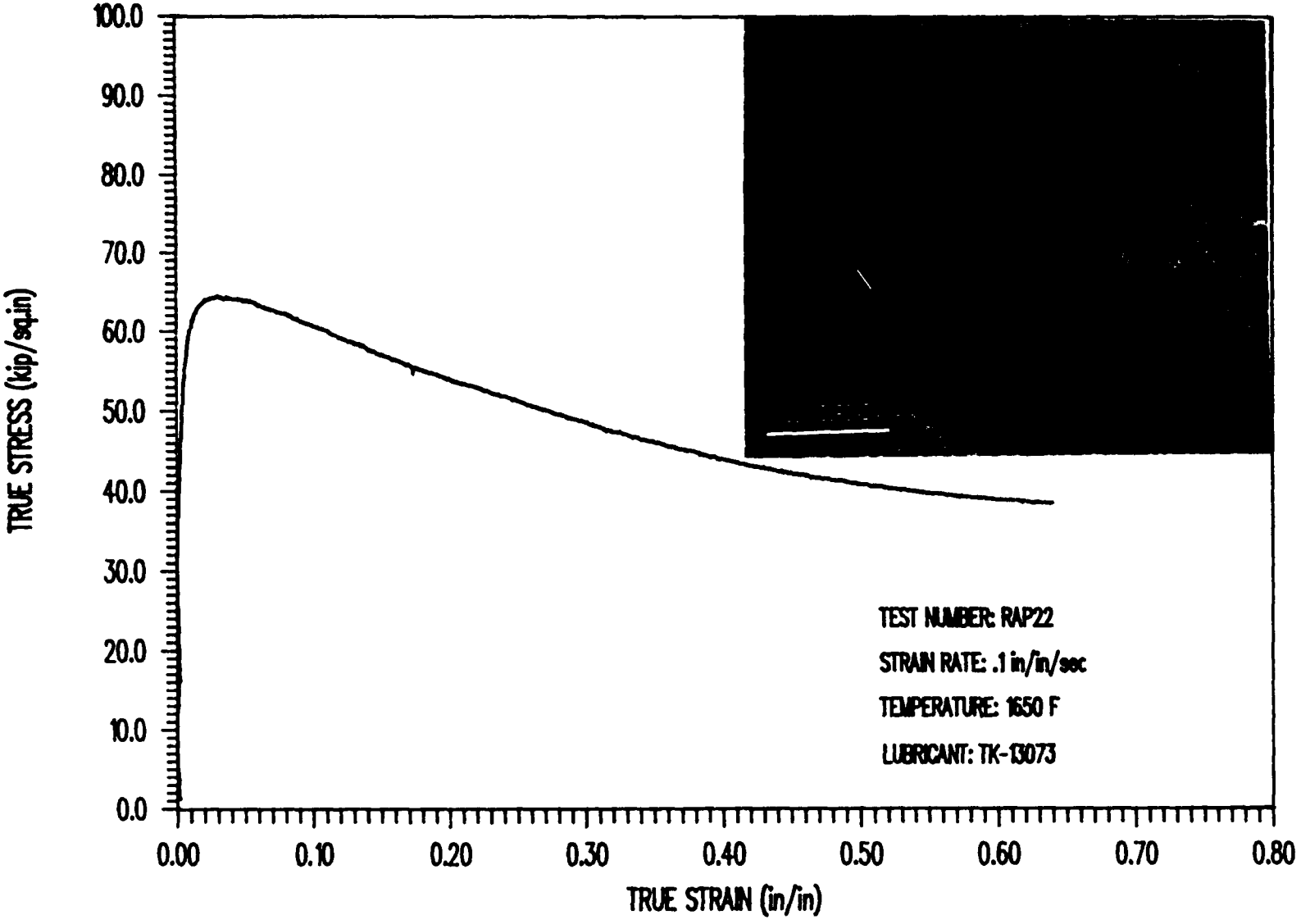

Figure 6. Compression true stress-true strain curve performed at 1650 F (899 C) and at a strain rate of $0.1s^{-1}$. The microstructure is a BEI view from the transverse axis of the specimen.

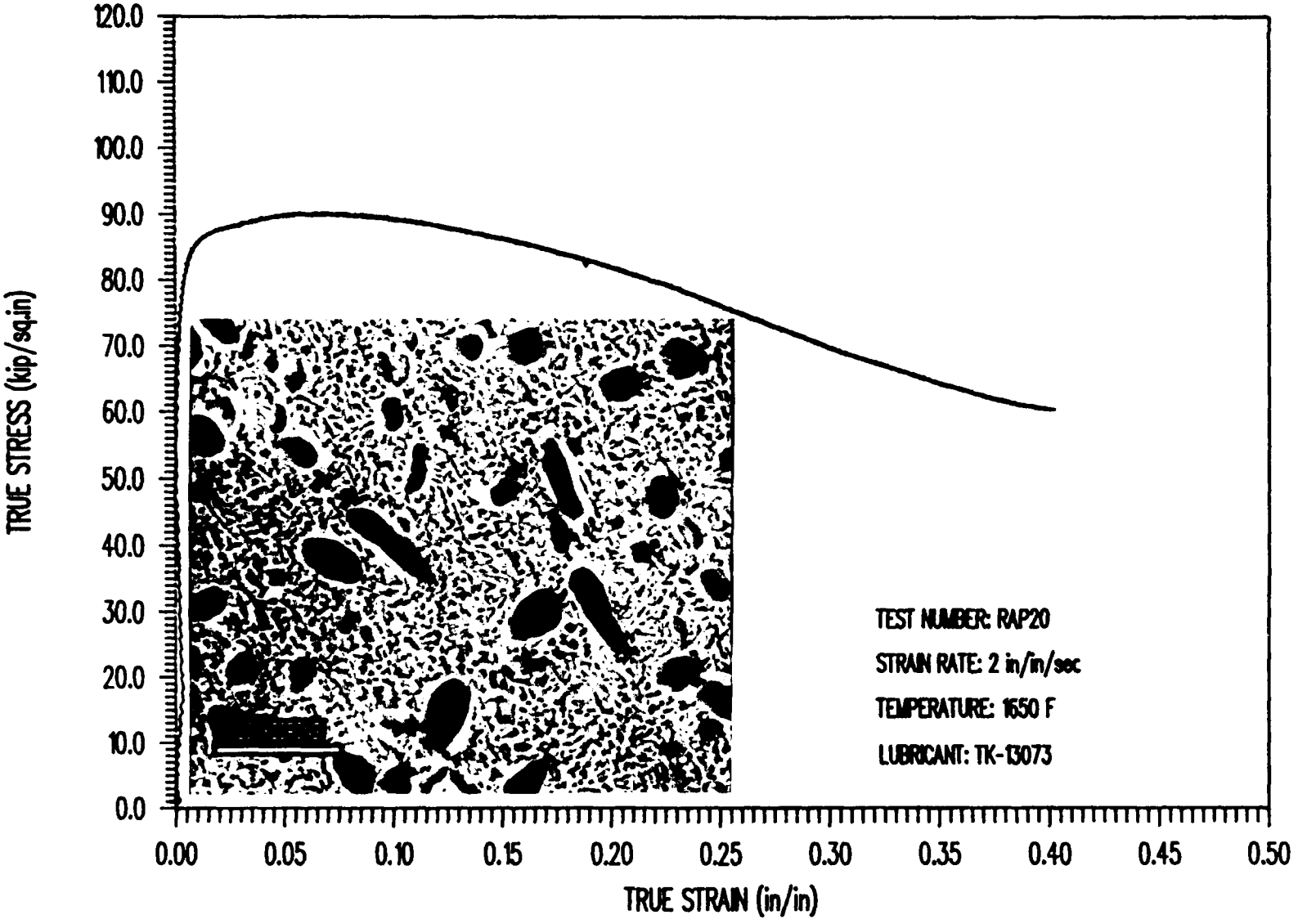

Figure 7. Compression true stress-true strain curve performed at 1650 F (899 C) and at a strain rate of 2.0 s^{-1}. The microstructure is a BEI view from the transverse axis of the specimen.

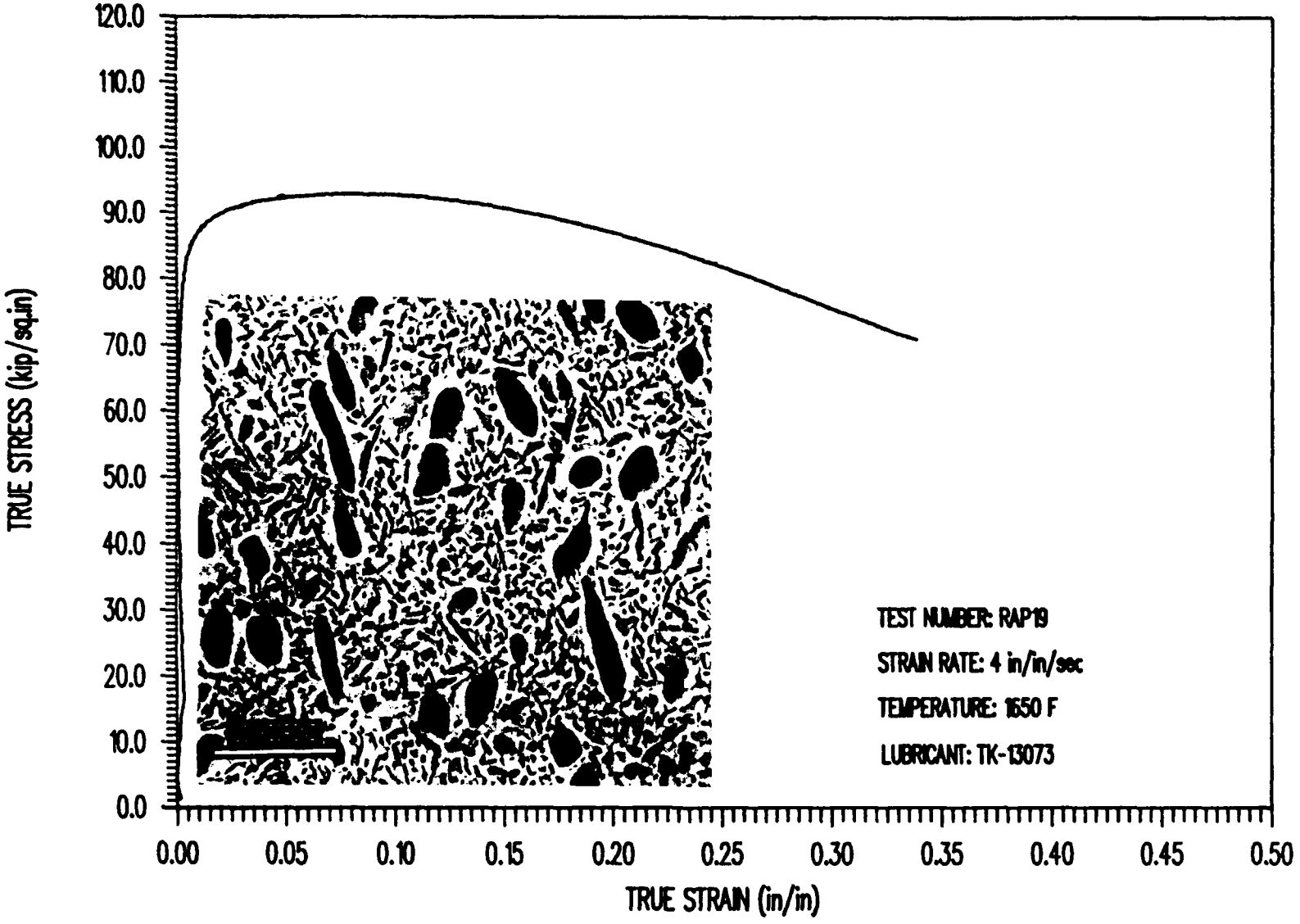

Figure 8. Compression true stress-true strain curve performed at 1650 F (899 C) and at a strain rate of 4.0 s^{-1}. The microstructure is a BEI view from the transverse axis of the specimen.

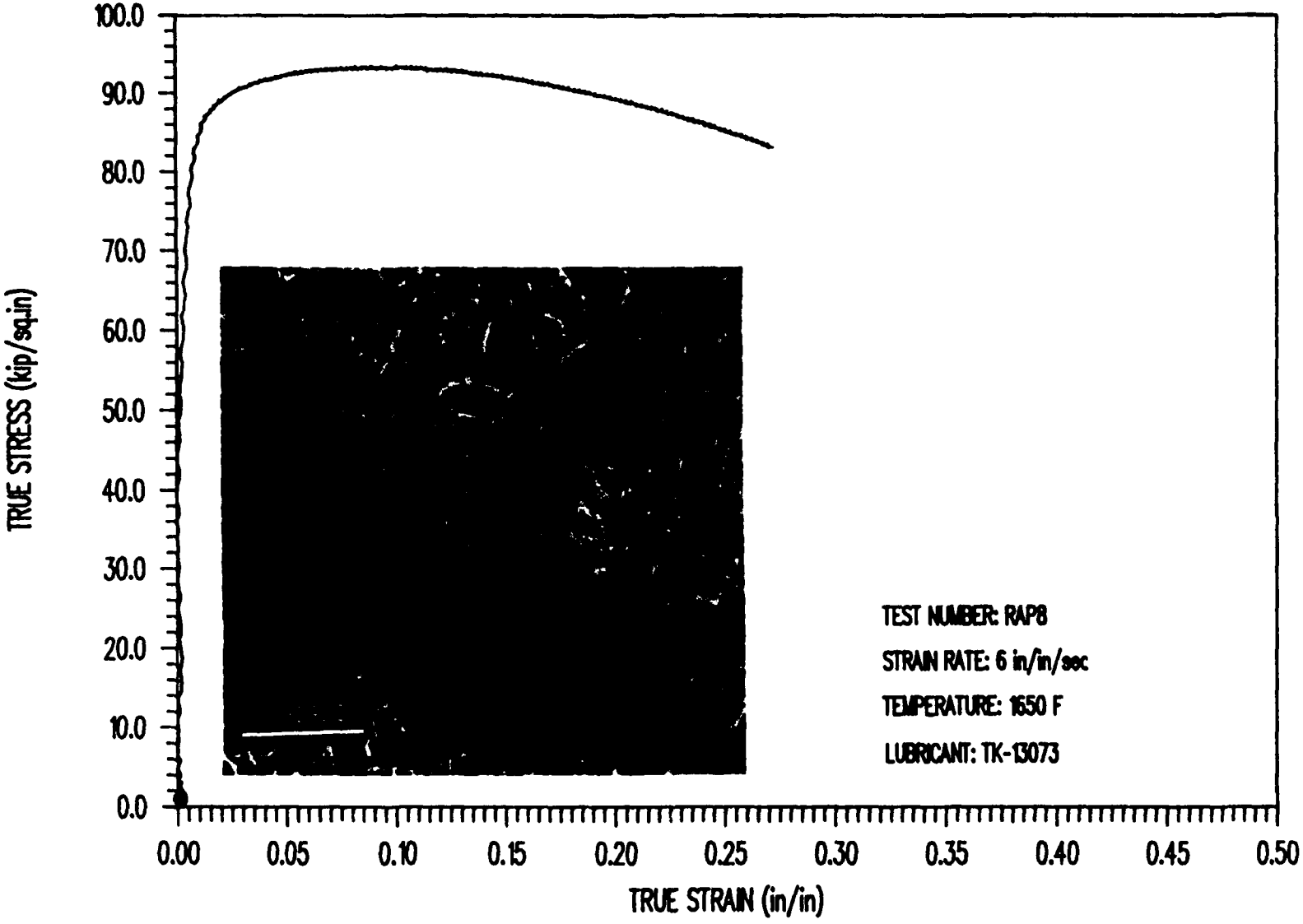

Figure 9. Compression true stress-true strain curve performed at 1650 F (899 C) and at a strain rate of 6.0 s^{-1}. The microstructure is a BEI view from the transverse axis of the specimen.

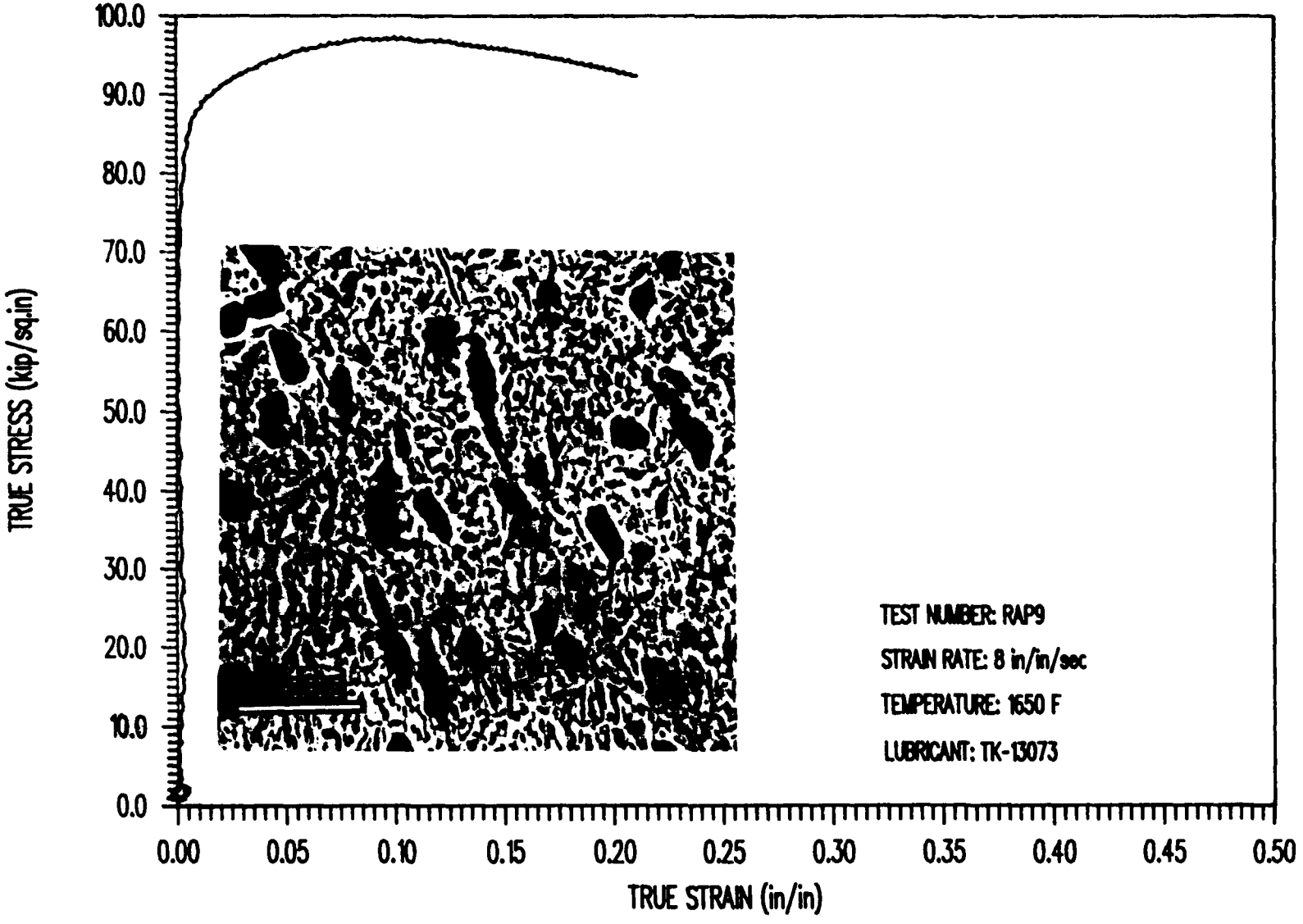

Figure 10. Compression true stress-true strain curve performed at 1650 F (899 C) and at a strain rate of 8.0 s^{-1}. The microstructure is a BEI view from the transverse axis of the specimen.

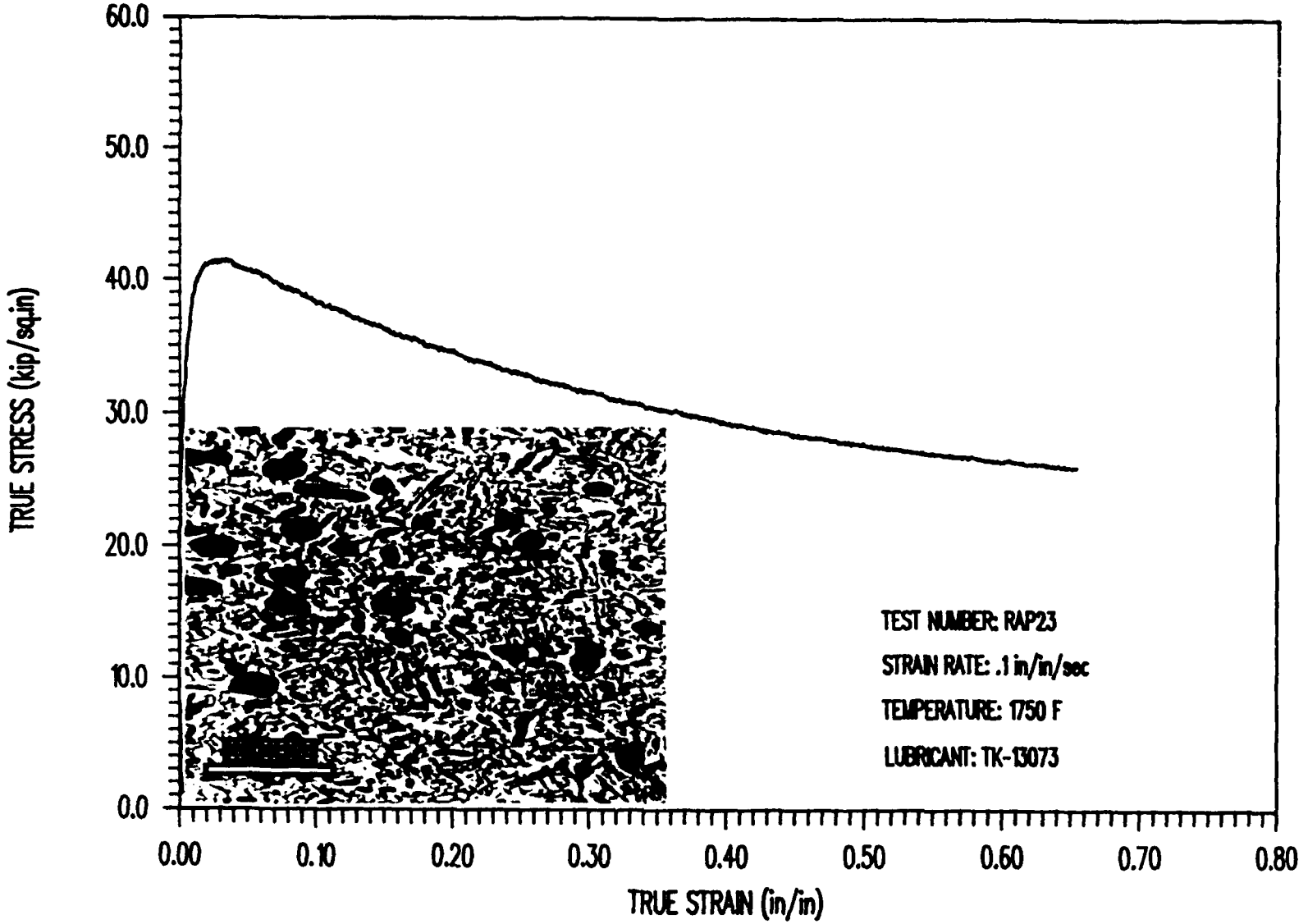

Figure 11. Compression true stress-true strain curve performed at 1750 F (954 C) and at a strain rate of 0.1 s^{-1}. The microstructure is a BEI view from the longitudinal axis of the specimen.

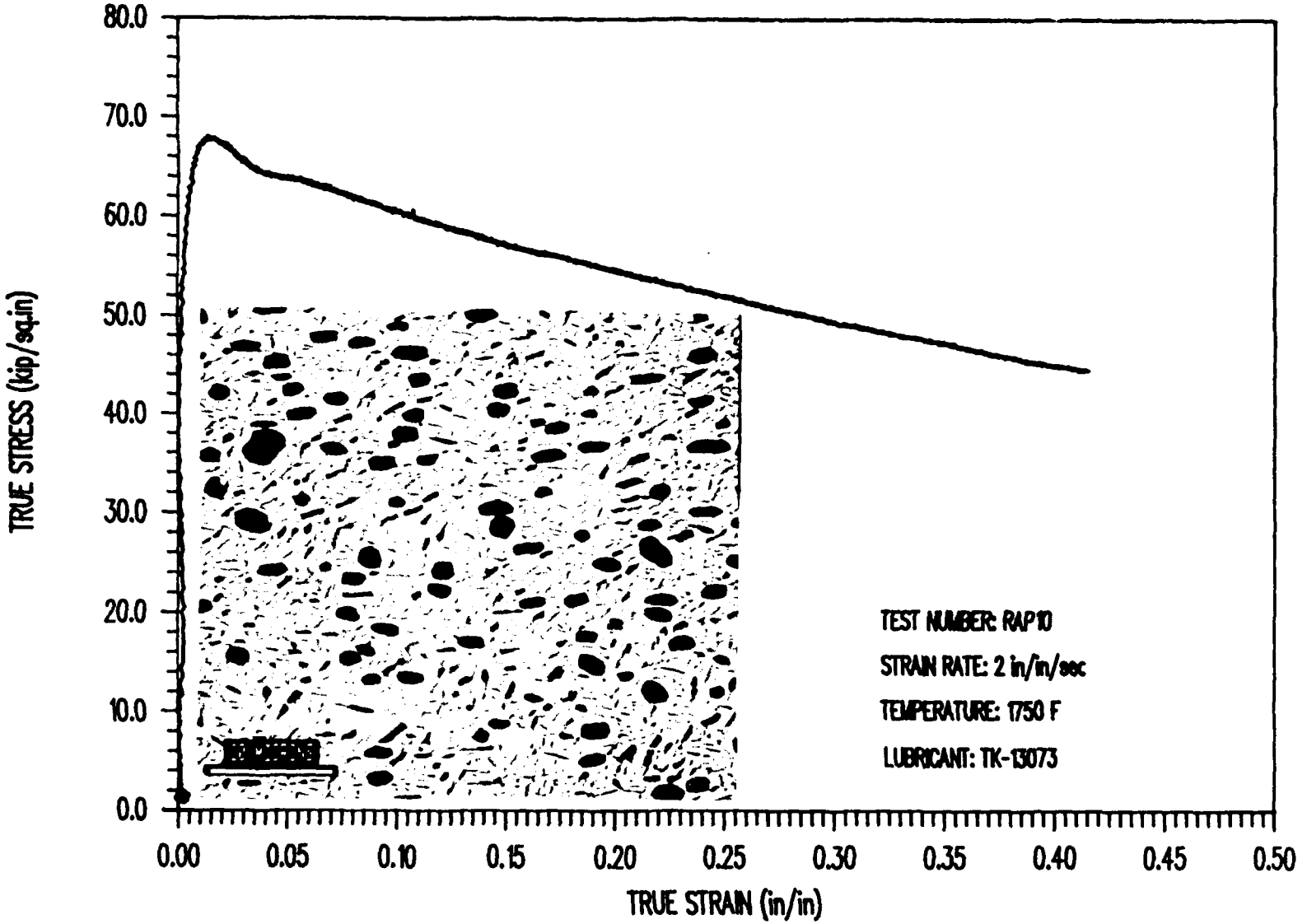

Figure 12. Compression true stress-true strain curve performed at 1750 F (954 C) and at a strain rate of 2.0 s^{-1}. The microstructure is a BEI view from the longitudinal axis of the specimen.

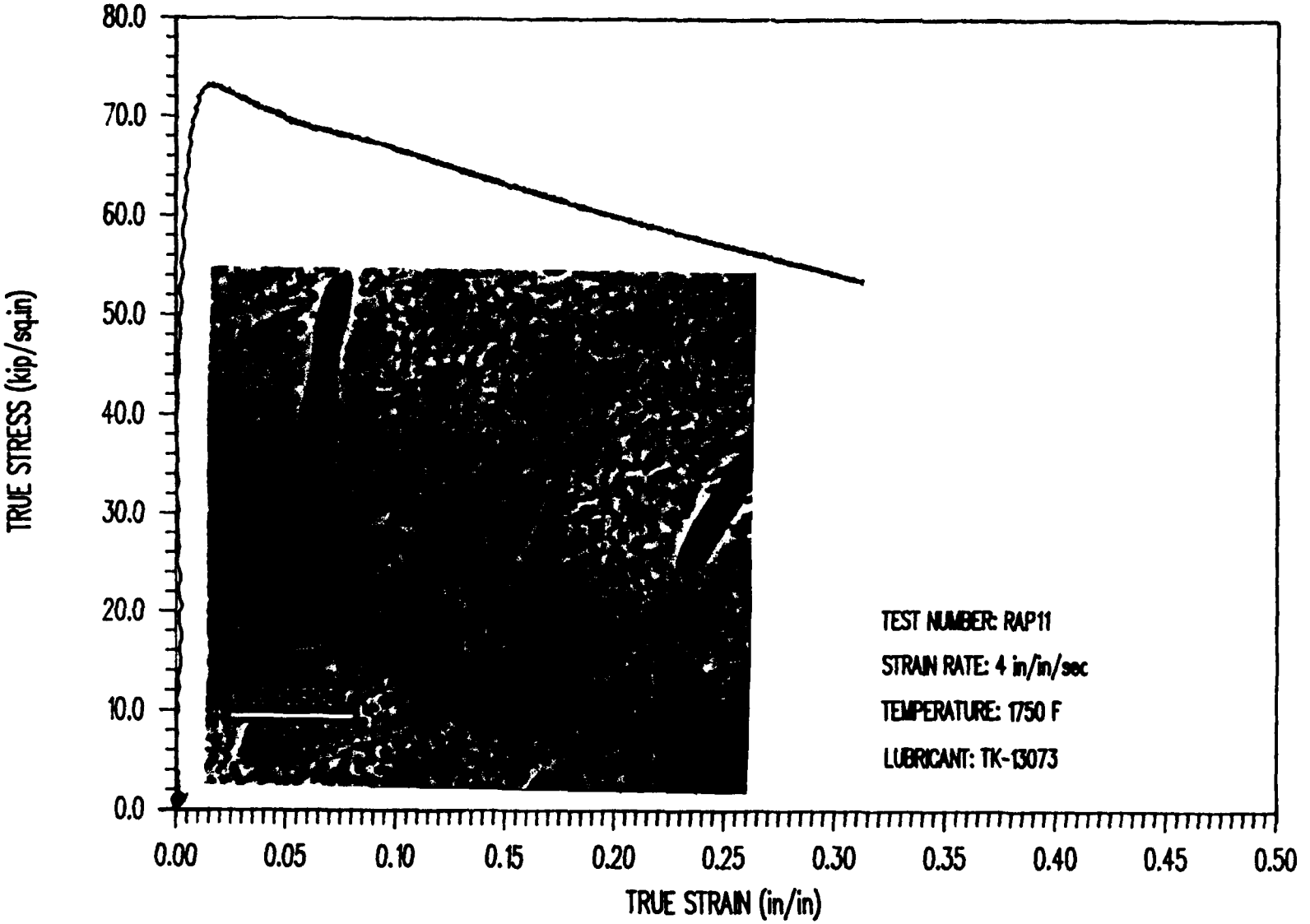

Figure 13. Compression true stress-true strain curve performed at 1750 F (954 C) and at a strain rate of 4.0 s-1. The microstructure is a BEI view from the transverse axis of the specimen.

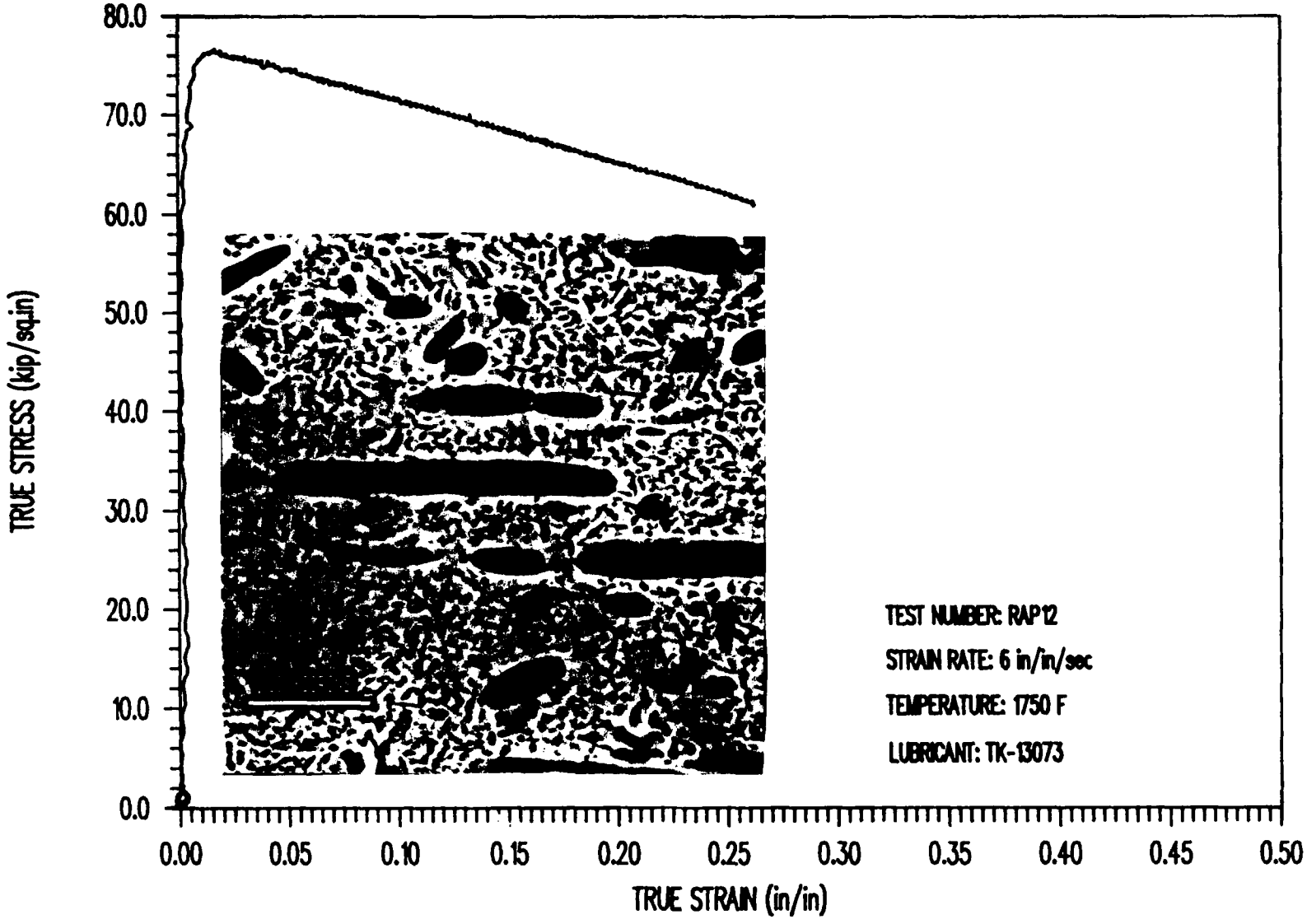

Figure 14. Compression true stress-true strain curve performed at 1750 F (954 C) and at a strain rate of 6.0 s^{-1}. The microstructure is a BEI view from the transverse axis of the specimen.

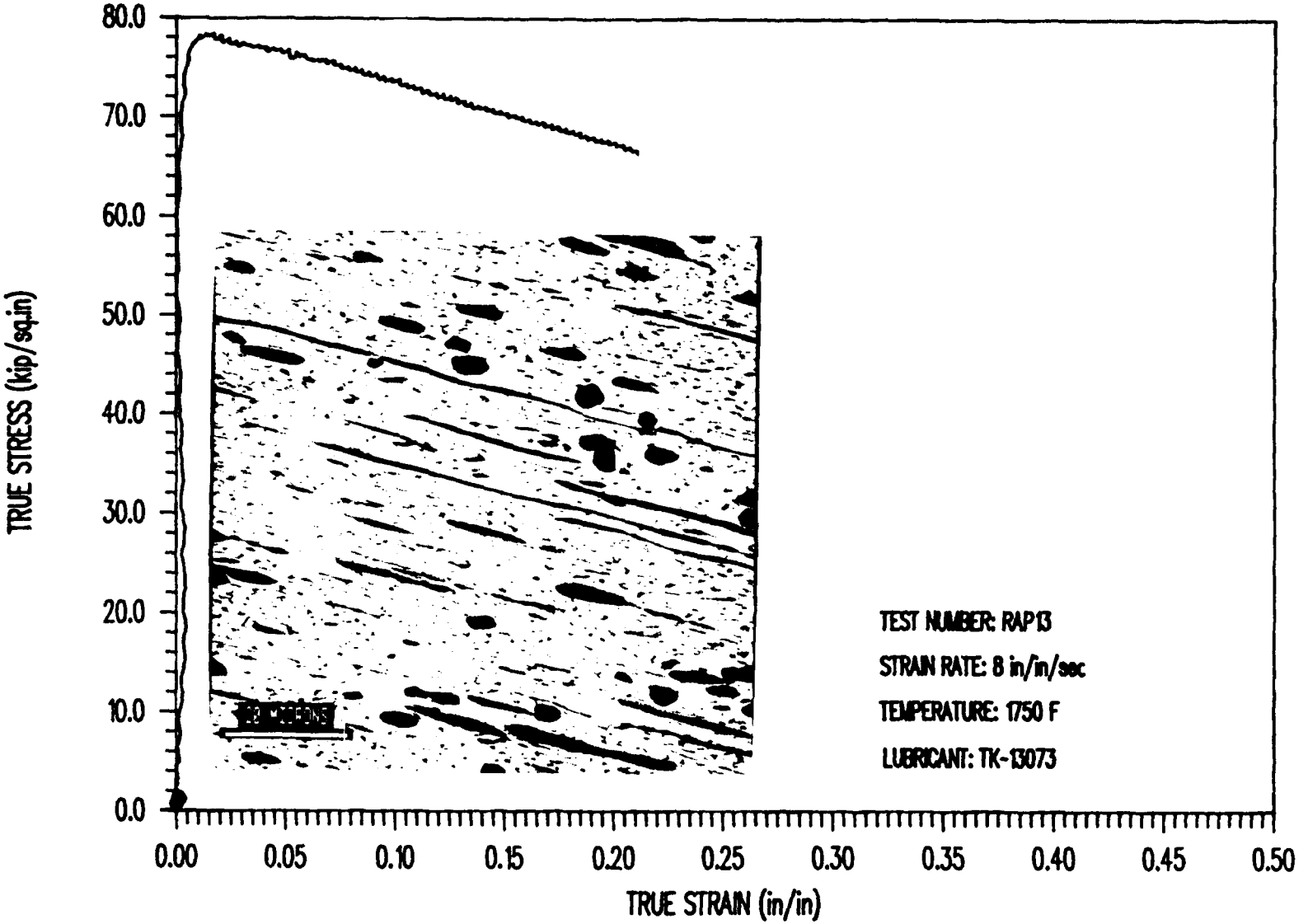

Figure 15. Compression true stress-true strain curve performed at 1750 F (954 C) and at a strain rate of 8.0 s-1. The microstructure is a BEI view from the longitudinal axis of the specimen.

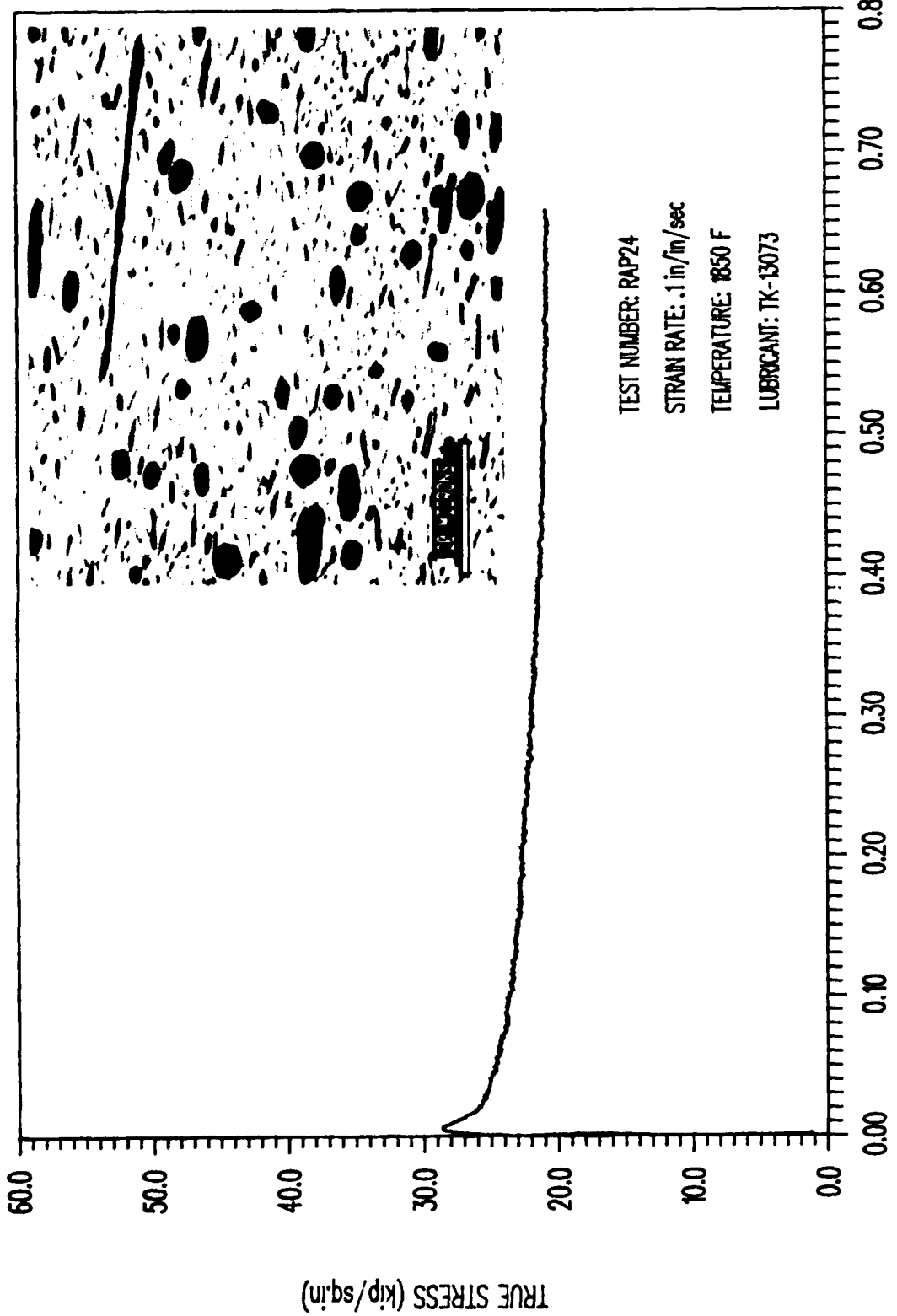

Figure 16. Compression true stress-true strain curve performed at 1850 F (1010 C) and at a strain rate of 0.1 s^{-1}. The microstructure is a BEI view from the longitudinal axis of the specimen.

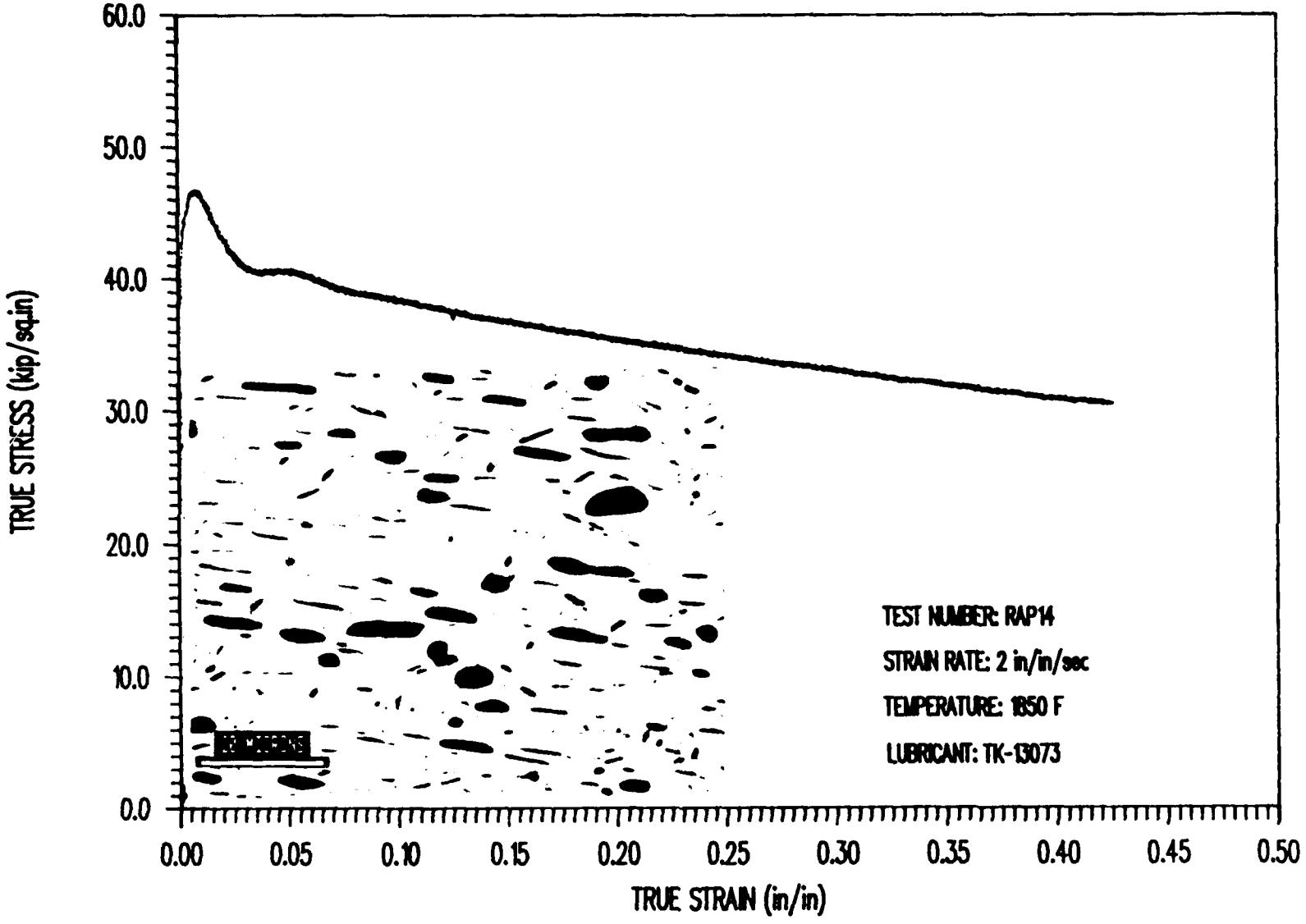

Figure 17. Compression true stress-true strain curve performed at 1850 F (1010 C) and at a strain rate of 2.0 s^{-1}. The microstructure is a BEI view from the longitudinal axis of the specimen.

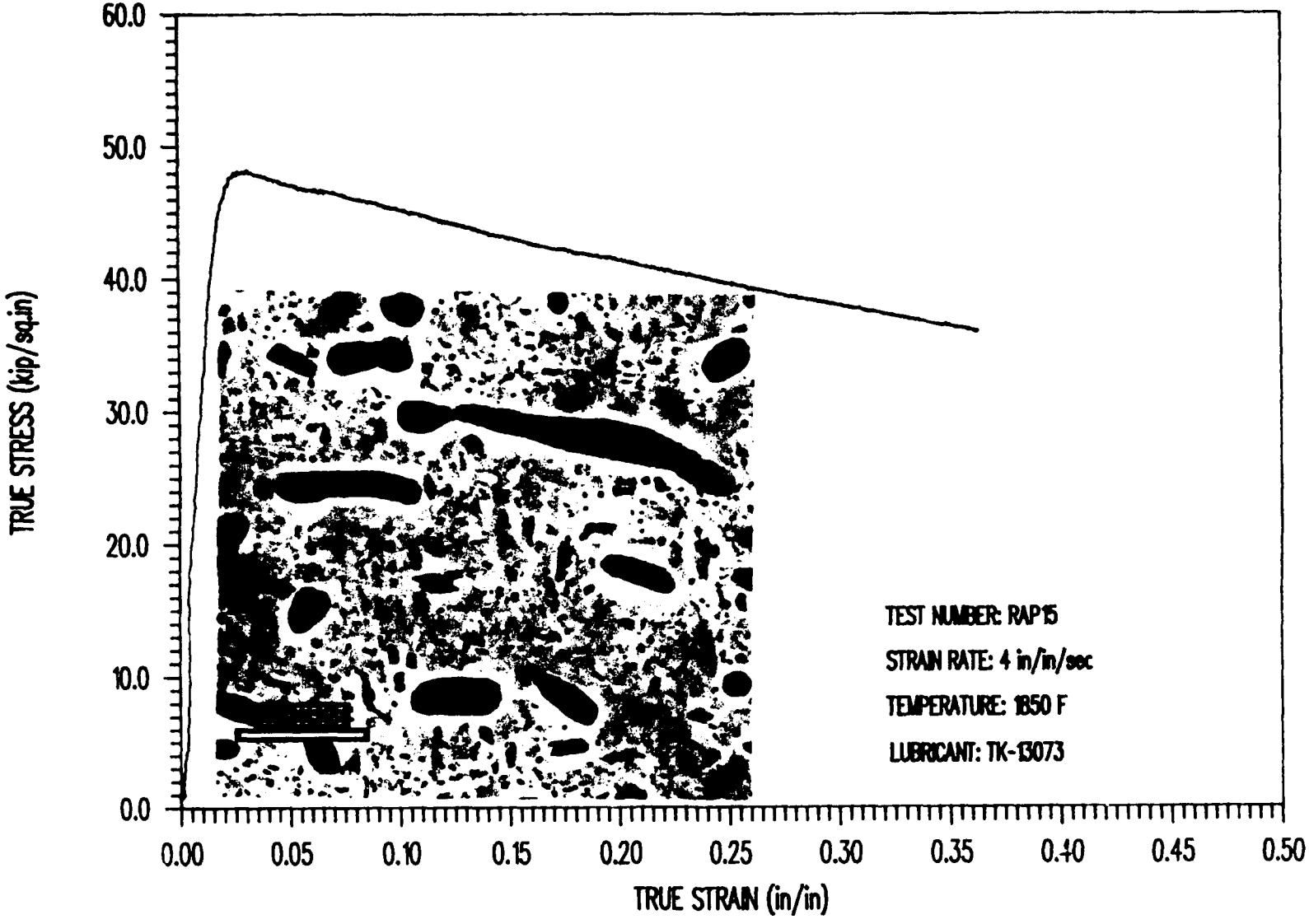

Figure 18. Compression true stress-true strain curve performed at 1850 F (1010 C) and at a strain rate of 4.0 s^{-1}. The microstructure is a BEI view from the transverse axis of the specimen.

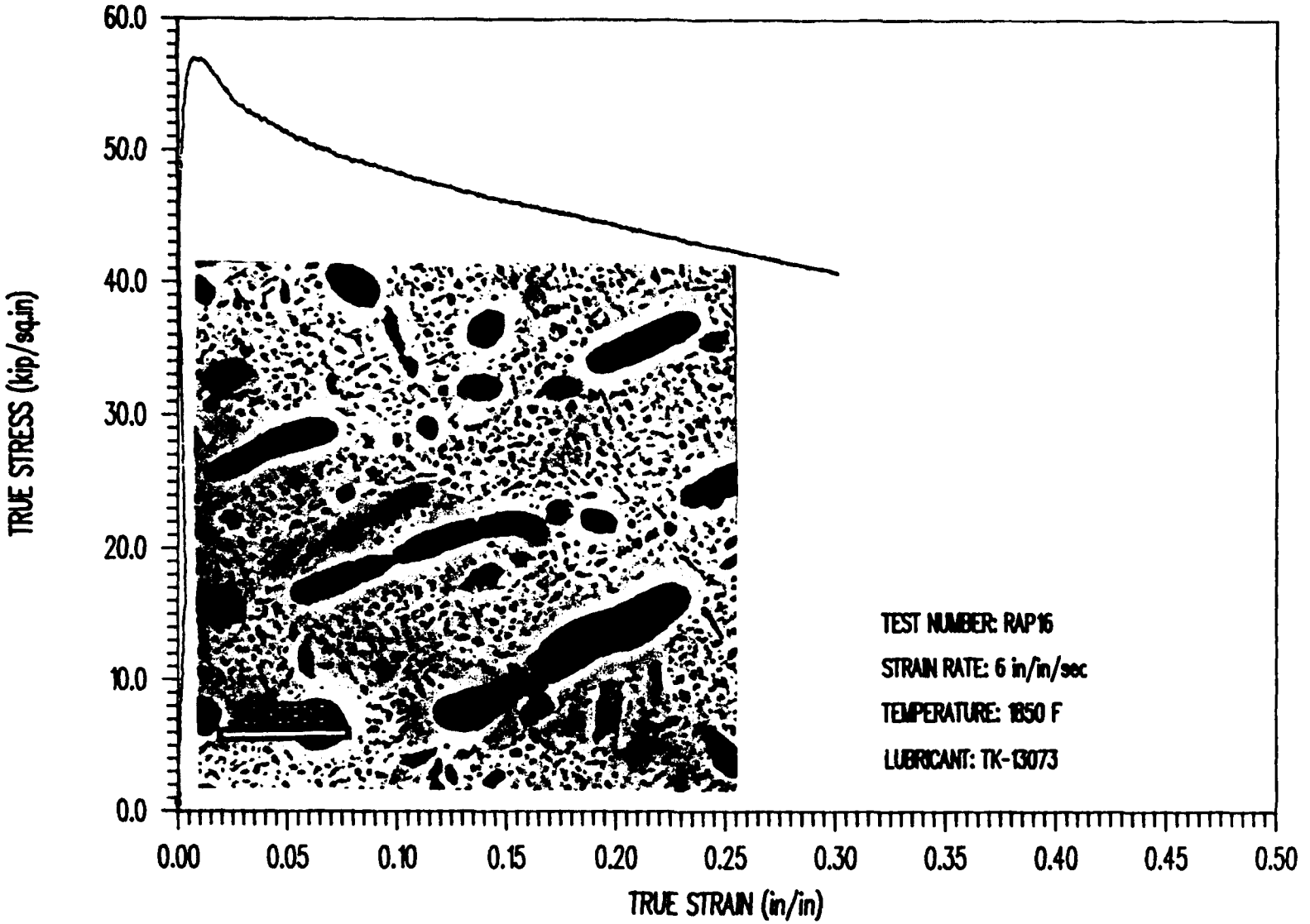

Figure 19. Compression true stress-true strain curve performed at 1850 F (1010 C) and at a strain rate of 6.0 s^{-1}. The microstructure is a BEI view from the transverse axis of the specimen.

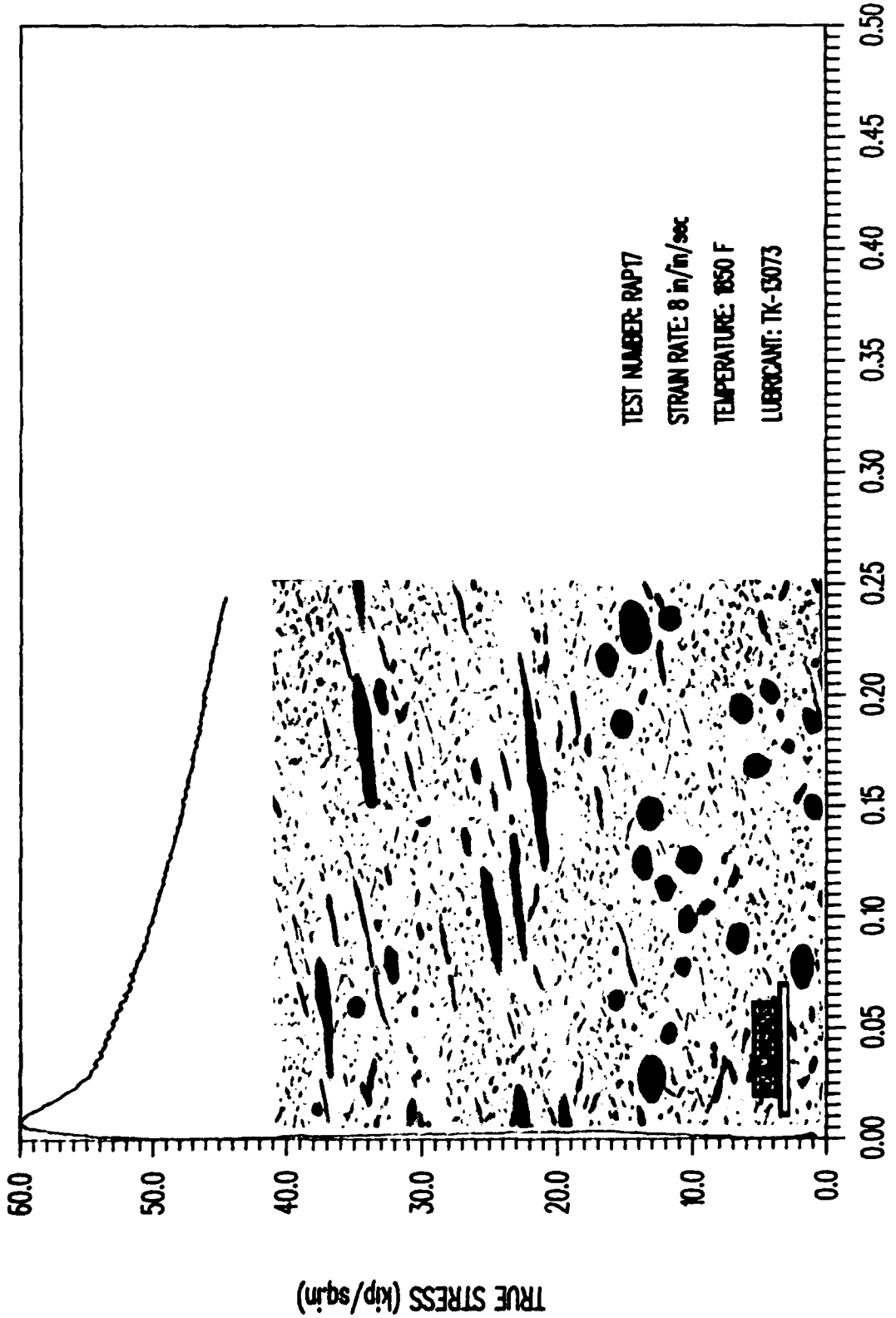

Figure 20. Compression true stress-true strain curve performed at 1850 F (1010 C) and at a strain rate of 8.0 s-1. The microstructure is a BEI view from the longitudinal axis of the specimen.

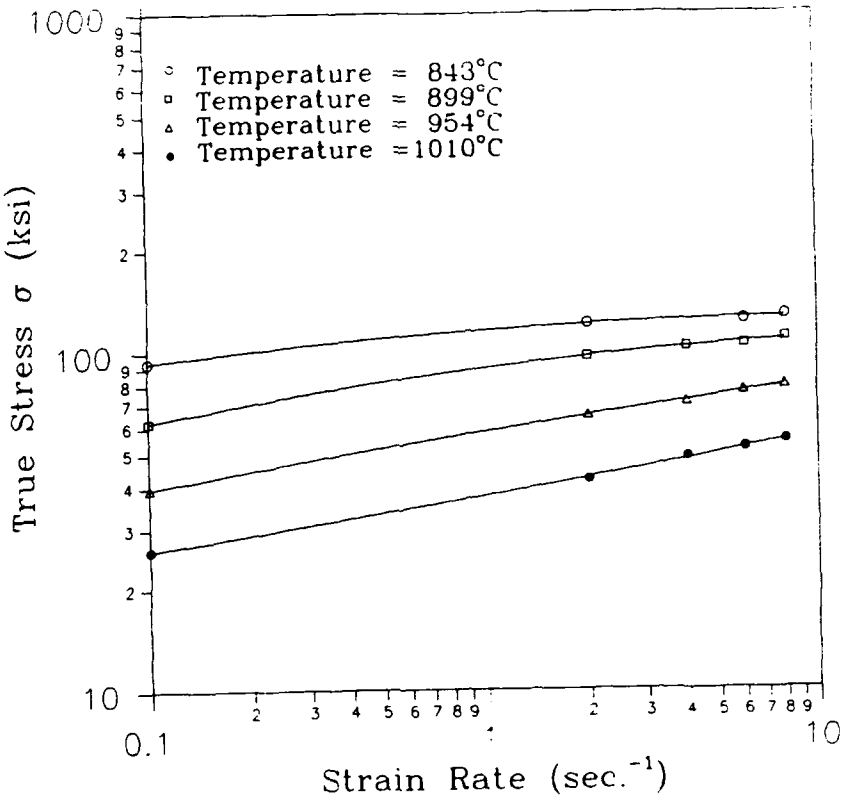

Figure 21. Effect of strain rate on stress in log-log scale at a true strain of 0.2.

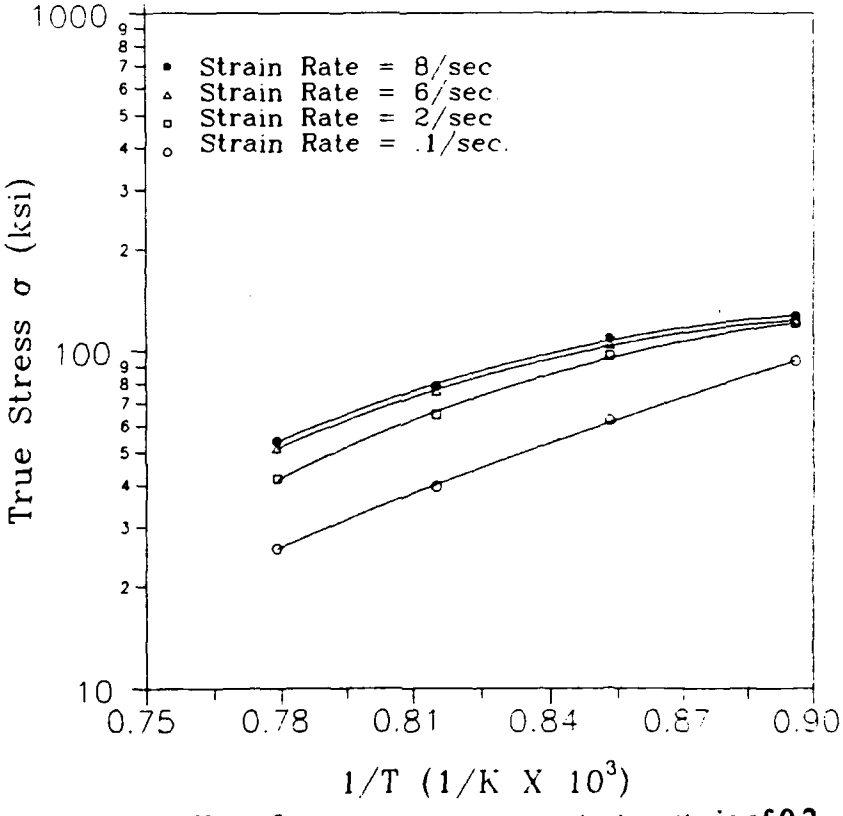

Figure 22. Effect of temperature on stress at a true strain of 0.2.

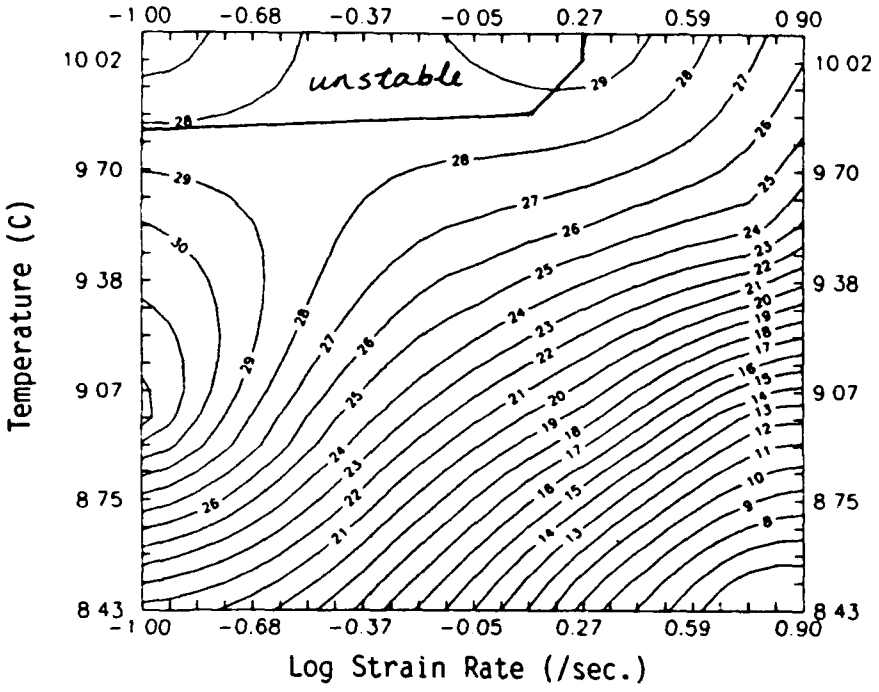

Figure 23. Processing map of Super α_2 at a true strain of 0.2.

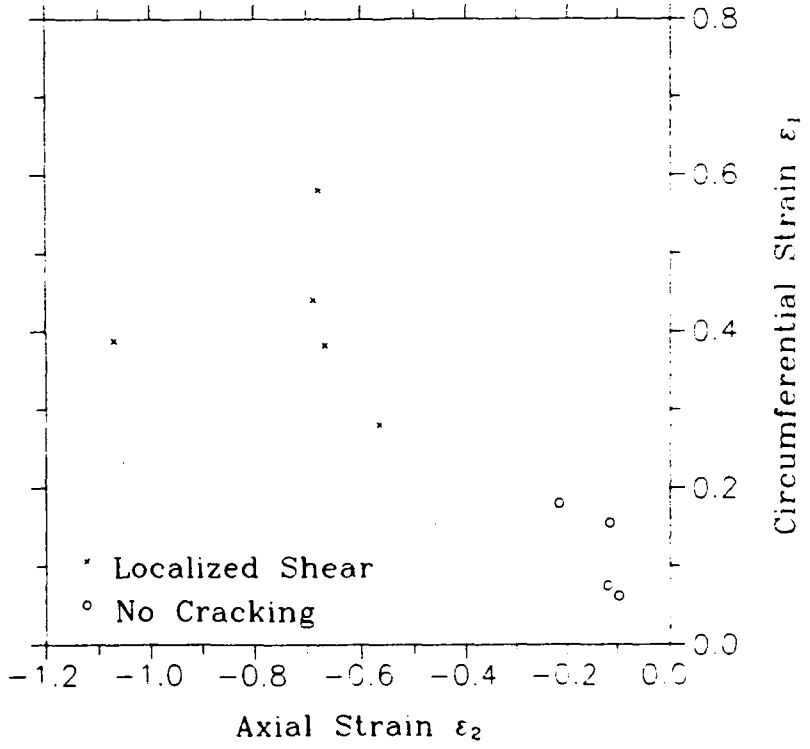

Figures 24. Workability of super α_2 at 843 C (1550 F).

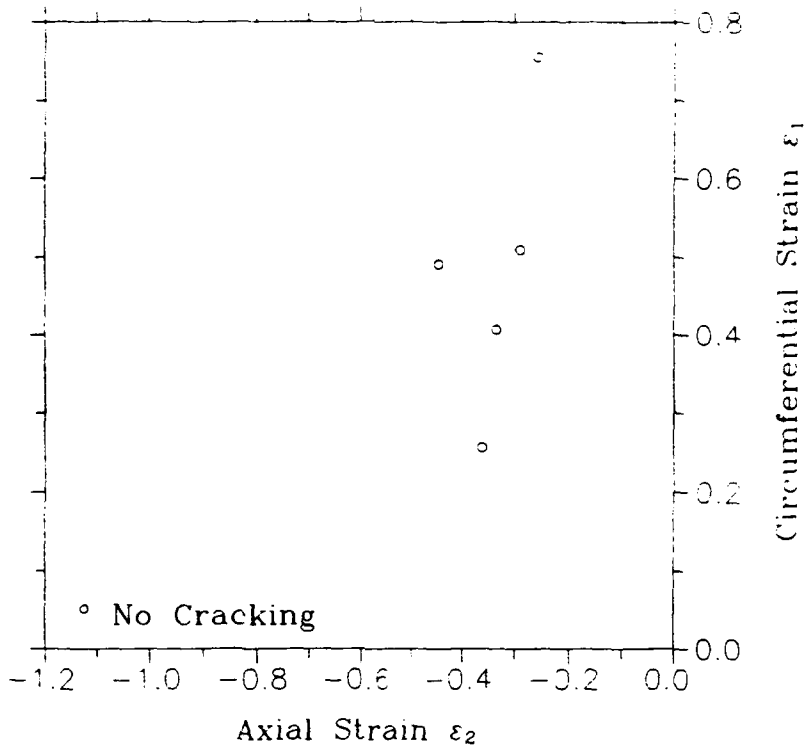

Figure 25. Workability of super α_2 at 1010 C (1850 F).

Summary

Compressive testing has been performed on super α_2 titanium aluminide over a range of temperatures and strain rates. The experimental conditions used in this work are representative of those used in conventional metalforming practices. From the stress-strain curves, the flow behavior was characterized and a map which indicates the optimum processing conditions was generated by employing the dynamic material modeling approach. The microstructure was characterized from the as-quenched specimens by SEM and are presented for each testing condition under the stress-strain curves. The testing was performed in the (α_2 + β)-field of the material, with the proportion of β–phase increasing with increase in temperature.

Implementation of Data Provided by the Atlas of Formability

The Atlas of Formability program provides ample data on flow behavior of various important engineering materials at different temperatures and strain rates. The data are valuable in design of metalforming processes with advanced materials. Microstructural changes with temperature and strain rates are also given in the Bulletin, which would help the design engineer to select processing parameters which lead to the desired microstructure.

The data can also be used to construct processing map with dynamic material modeling approach, giving stable and unstable regions in terms of temperature and strain rate. The temperature and strain rate at the highest efficiency in the stable region provide the optimum processing condition. In some metalworking processes such as forging, the final strain and strain rate vary at different position in the work piece. An analysis of the process with FEM can ensure that the strain rates at the processing temperature in the whole workpiece fall into the stable regions in the processing map. Furthermore, FEM analysis with the data from the Atlas of Formability can also be coupled with fracture criteria to predict defect formation in metalworking processes.

Using the data provided by the Atlas of Formability, FEM design of metalforming processes, dynamic material modeling, defect prediction in forming processes, microstructure characterization of deformed materials are common practice in Concurrent Technologies Corporation. Any needs in solving problems in metalworking processes can be directed to Dr. Prabir K. Chaudhury, Manager of the Atlas of Formability project, at (814) 269-2594.